SCIENCE CHINA
Physics, Mechanics & Astronomy

• Article •

December 2017 Vol. 60 No. 12: 124711
doi: 10.1007/s11433-017-9072-8

β-distribution for Reynolds stress and turbulent heat flux in relaxation turbulent boundary layer of compression ramp

YanChao Hu, WeiTao Bi, ShiYao Li, and ZhenSu She*

State Key Laboratory for Turbulence and Complex Systems and Department of Mechanics and Engineering Science, College of Engineering, Peking University, Beijing 100871, China

Received April 28, 2017; accepted June 13, 2017; published online September 11, 2017

A challenge in the study of turbulent boundary layers (TBLs) is to understand the non-equilibrium relaxation process after separation and reattachment due to shock-wave/boundary-layer interaction. The classical boundary layer theory cannot deal with the strong adverse pressure gradient, and hence, the computational modeling of this process remains inaccurate. Here, we report the direct numerical simulation results of the relaxation TBL behind a compression ramp, which reveal the presence of intense large-scale eddies, with significantly enhanced Reynolds stress and turbulent heat flux. A crucial finding is that the wall-normal profiles of the excess Reynolds stress and turbulent heat flux obey a β-distribution, which is a product of two power laws with respect to the wall-normal distances from the wall and from the boundary layer edge. In addition, the streamwise decays of the excess Reynolds stress and turbulent heat flux also exhibit power laws with respect to the streamwise distance from the corner of the compression ramp. These results suggest that the relaxation TBL obeys the dilation symmetry, which is a specific form of self-organization in this complex non-equilibrium flow. The β-distribution yields important hints for the development of a turbulence model.

compression ramp, relaxation turbulent boundary layer, Reynolds stress, β-distribution, symmetry

PACS number(s): 47.27.Nz, 47.40.Ki, 47.40.Nm, 47.85.Gj

Citation: Y. C. Hu, W. T. Bi, S. Y. Li, and Z. S. She, β-distribution for Reynolds stress and turbulent heat flux in relaxation turbulent boundary layer of compression ramp, Sci. China-Phys. Mech. Astron. **60**, 124711 (2017), doi: 10.1007/s11433-017-9072-8

1 Introduction

Equilibrium turbulent boundary layers (TBLs), including canonical TBLs on a flat plate with zero pressure gradient, and those with the so-called equilibrium pressure gradients [1,2], are characterized by wall-normal mean profiles varying only with the local quantities (velocity and length), independent of the flow history. In contrast, non-equilibrium TBLs are more frequently encountered when the flows are subjected to strong disturbances such as separations and shocks. Subsequent relaxations towards equilibrium flows form so-called relaxation TBLs, where there are often intense fluctuations inherited from upstream, and redistributed and dissipated afterwards, balanced by a large adverse pressure gradient. In general, the relaxation TBLs are non-equilibrium and cannot be described by the classical boundary layer theory. The turbulence models, whose closure forms and parameters are optimized for canonical flows, thus yield poor predictions for the relaxation TBLs [3].

For obvious engineering interests, relaxation TBLs have been investigated for several decades [4]. Various disturbances have been studied, including separation and reattachment induced by protruding obstacles [5-7], pressure gradients [8], shock-wave/boundary-layer interactions [9, 10], and variations in boundary conditions such as curvature [11], roughness [12-14], micro vortex generators [15], wall tem-

*Corresponding author (email: she@pku.edu.cn)

perature [16, 17], and blowing or suction [18]. In these studies, the main focus is on the response and development of the mean profiles, as well as the flow structures, to identify the differences and similarities among various perturbations. As concluded in the review by Smits and Wood [4], these studies suggest extra requirements for turbulence models in more complex flow conditions.

Compared to efforts made in collecting data and carrying out empirical analyses of non-equilibrium TBLs, the theoretical framework is lacking. The difficulty lies in the complexity of the response and relaxation processes in the presence of many physical factors [4]. Here, we carry out a direct numerical simulation (DNS) study of the relaxation TBLs in compression ramps with varying angles, and report the discovery of surprisingly simple distributions of the Reynolds stress and turbulent heat flux when a canonical flow component is subtracted out. A symmetry-based argument [19-25] is employed to predict the form of the distributions, a β-distribution. Furthermore, their magnitudes exhibit power law scaling with respect to the streamwise distance from the corner of the compression ramp. The results suggest that the relaxation TBL obeys the dilation symmetry, which is a specific form of the self-organization in this non-equilibrium flow, and the β-distribution can be used for the development of the turbulence model. Note that the symmetry-based idea has been successfully implemented for modeling the natural and bypass transitions in TBLs [26], which are well-known to be in non-equilibrium.

The paper is organized as follows. Sect. 2 explains the DNS details and the general features of the flows behind the compression ramp. Sect. 3 presents the results, including the Reynolds stress and turbulent heat flux distributions in the relaxation TBLs, their β-distributions, and the streamwise development. Sect. 4 contains discussions and conclusions.

2 DNS details and flow features

The DNS of compression ramps has been conducted with an open-source full Navier-Stokes solver called OpenCFD, developed by Li et al. [27] at the Institute of Mechanics of Chinese Academy of Sciences for the scientific computation of spatially-developing compressible turbulent flows. A laminar incoming boundary layer flow with Mach number 2.9 is perturbed by blowing and suction disturbances to induce a transition, and then a fully-developed turbulent state finally reaches a Reynolds number (Re_θ = 2344) [28,29] around the ramp corner, where the shock-wave/boundary-layer interaction occurs. Three ramps (case A14, A20 and A24) are simulated at inclination angles of 14°, 20° and 24°. They induce shock waves of different strengths and generate separations of different sizes. Behind the compression corner, the TBL relaxes to form the relaxation TBL, before flowing out of the simulation domain.

The three simulations have similar domains with similar computational meshes. As shown in Figure 1, the extension of the flat plate is from −335 mm to 0 mm, and of the ramp from 0 mm to 50 mm along the ramp surface, where the origin is chosen to be at the ramp corner. The wall-normal extension is 35 mm and the spanwise extension is 14 mm. The mesh number is 2160 × 160 × 140. Following the convention, the dense mesh is set in the corner region at −35 mm≤ x ≤ 35 mm and near the wall, and is uniform in the spanwise direction. Characteristic mesh resolutions for the 24° ramp, for example, are: $\Delta x^+ \approx 4.0$, $\Delta y_w^+ \approx 0.5$ and $\Delta z^+ \approx 5.0$ (superscript plus denotes wall unit normalization) before the separation.

The inlet is a two-dimensional supersonic laminar boundary layer located at the 200 mm downstream leading edge of a flat-plate. Two-dimensional laminar results, obtained with the same grid and inflow conditions as the turbulent calculations, are selected as the initial conditions. A non-reflecting boundary condition is used for both the upper boundary and outlet, and a periodic boundary condition is used in the spanwise direction. Non-slip and isothermal ($T_w = 2.84T_\infty$) wall conditions are used for the flat plate and ramp surface, except within −305 mm< x < −285 mm on the wall where there is a non-zero distribution of the wall-normal velocity set as the blowing and suction disturbances, following Pirozzoli et al. [30].

In the simulation, spatial coordinate is normalized to 1 mm and the other quantities are normalized with respect to the

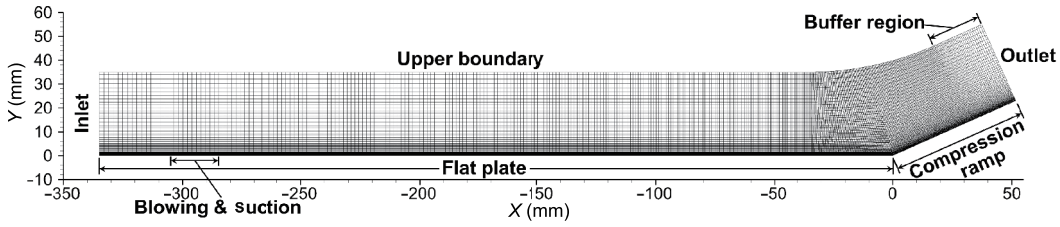

Figure 1 Illustration of the computational domain and mesh.

corresponding free-stream values. Dimensionless Navier-Stokes equations are solved with finite difference algorithms in curvilinear coordinates. The convective flux terms are computed by the Steger-Warming splitting method and discretized using the WENO-SYMBO method of Martín et al. [31]. The viscous flux terms are discretized with the eighth-order central difference scheme. An explicit third-order total variation diminishing (TVD)-type Runge-Kutta method is used for the time evolution. The mean quantities (profiles) are obtained by averaging in time and in the spanwise direction. Snapshots are also acquired for visualizing instantaneous flow structures.

The 24° ramp case has been measured experimentally by Bookey et al. [32] and computed by Wu et al. [33] and Li et al. [28,29] with DNSs. Figures 2 and 3 compare the skin friction coefficient and mean wall pressure distributions of the current DNS with those of previous studies [28, 31, 32, 34], which show that the current simulation is reasonably accurate.

Figure 4 is a numerical Schlieren visualization of the instantaneous flow structures in the corner region. A canonical

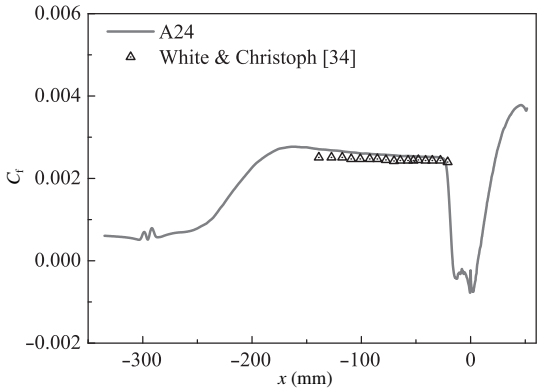

Figure 2 Skin friction coefficient distribution for the 24° ramp denoted by A24. See Figure 4 for the definition of x.

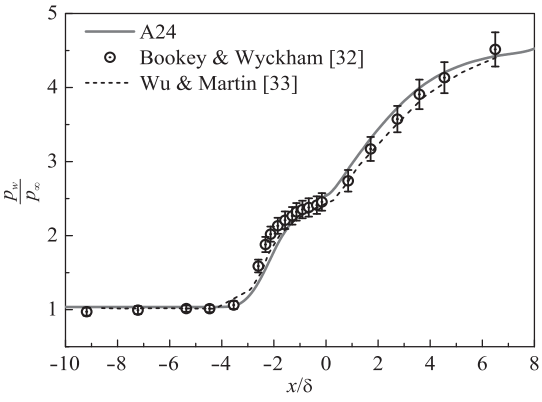

Figure 3 Mean wall pressure distribution for the 24° ramp. δ is the boundary layer thickness at x=–35 mm.

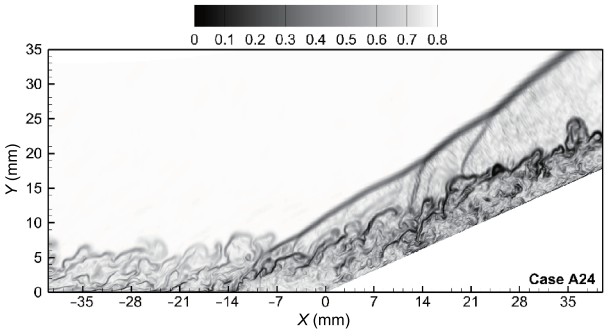

Figure 4 Numerical Schlieren visualization of instantaneous flow structures in the corner region of the 24° ramp.

TBL develops before reaching the corner, and the flow deflects near the corner, generating a strong shock wave with an abrupt pressure rise (Figure 3), and inducing a separation around the corner. The vortexes in the TBL penetrate the oblique shock wave [35] and shed into the flow interior, and then reattach to the ramp, resulting in strong turbulent fluctuations in the bulk of the subsequent relaxation TBL.

The above observations can be further validated by examining the mean-field contours. Figure 5 exhibits the spatial distributions of the mean pressure, mean temperature, turbulent kinetic energy, and temperature fluctuation intensity for the 24° ramp. Basically, we can divide the flow field into three regions: the equilibrium incoming TBL, the corner region with intense shock-wave/boundary-layer interaction, and the relaxation TBL. From Figure 5(a) one finds that the incoming TBL is undisturbed before $x = -21$ mm for the 24° ramp; from Figure 5(b)-(d) one finds that a quasiparallel flow is reestablished (such that the boundary layer approximation is applicable) after the reattachment location at about $x = 7$ mm (see Figure 5(b)). The latter is set to be the beginning of the relaxation TBL, which will be the focus of the subsequent study. The relaxation TBL is significantly different from the incoming equilibrium TBL in several aspects. First, a strong streamwise adverse pressure gradient develops throughout the relaxation process. The isopressure lines are curved in the wall-normal direction, revealing a strong wall-normal velocity fluctuation to balance the mean pressure variation. Second, compared with those of the incoming TBL, the mean temperature, turbulent kinetic energy, and temperature fluctuation intensity are significantly enhanced in the bulk (i.e., away from the near-wall region) of the relaxation TBL; in particular, the latter two fluctuation intensities occupy the bulk flow. We believe that this turbulence is the result of two processes, one from the shock-wave/boundary-layer interaction shedding from the corner region, and the other from the adverse pressure gradient formed globally. Below, a quantitative model will be developed based on this understanding.

Figure 6(a) visualizes this turbulence with vortical structures extracted by the common Q criterion for the 24° ramp

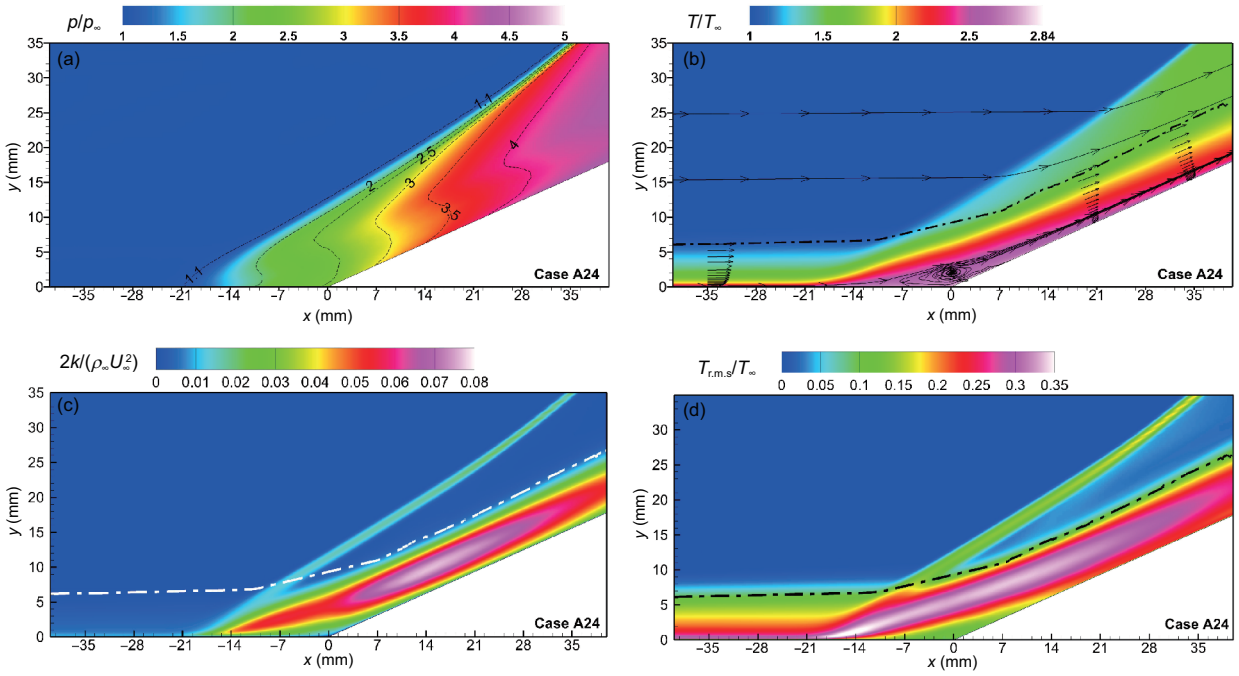

Figure 5 (Color online) Contours of (a) mean pressure, (b) mean temperature together with streamlines and mean velocity vectors ahead of and behind the corner, (c) turbulent kinetic energy, and (d) temperature fluctuation intensity, for the 24° ramp. The dash-dot lines in (b)-(d) denote the location of the boundary layer thickness (i.e., δ_{99}).

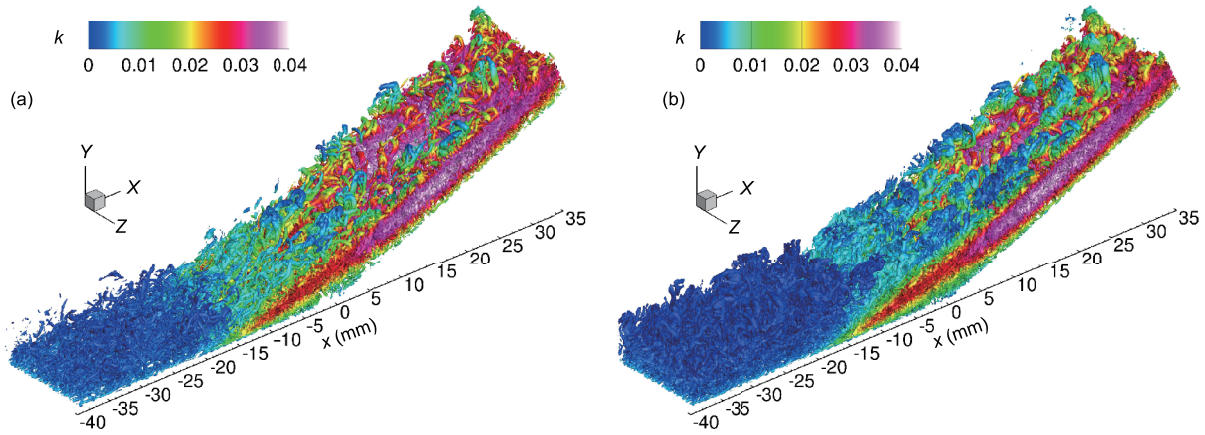

Figure 6 (Color online) Instantaneous vortical structures extracted by the Q criterion (a) and Ω criterion (b) for the 24° ramp. The colors show the magnitude of the turbulent kinetic energy.

at $Q = 0.05$. Indeed, one sees a crowd of intense large-scale eddies in the bulk of the relaxation TBL, which are much stronger, bigger, and much more energetic than those in the incoming equilibrium TBL. Because the Q criterion may give different vortical structures when the threshold is changed, we also use the recently reported Ω method [36] to extract the vortex structures. In Figure 6(b) both small and large vortexes are captured by the Ω method and the vortexes on the ramp remain more energetic. These energetic eddies significantly distort the mean fields of the relaxation TBL (see Figure 5(b) for the mean velocity distortion) and present new challenges for the theoretical approach beyond the classical boundary layer theory.

The mechanism for the turbulence intensification due to shock-wave/boundary-layer interactions has been widely discussed in the literature [4, 37, 38]. Anyiwo and Bushnell [39] and Zang et al. [40] pointed out that the shock wave can amplify turbulence through its oscillations and the jump condition. Settles et al. [41] and Ardonceau [42] found that longitudinal roll-cells may be formed to produce three-dimensional effects, which contribute as well. Here, the shock wave indeed oscillates significantly, and induces mas-

sive separations, contributing to the remarkable turbulence enhancement.

3 Results

3.1 Reynolds stress and turbulent heat flux profiles

The main concerns of this study are the description of the streamwise development of the Reynolds stress and turbulent heat flux in the relaxation TBL, owing to their paramount importance in turbulence modeling. As shown in Figure 4, the relaxation TBL remains quasiparallel along the ramp surface. Therefore, the Reynolds stress is $-\bar{\rho}\widetilde{u''v''}$ (denoted by W_{uv} hereinafter) and the turbulent heat flux, $-C_p\bar{\rho}\widetilde{T''v''}$ (denoted by W_Θ hereinafter), where ρ is the density, T is the temperature, C_p is the specific heat at constant pressure, and u and v are the streamwise and wall-normal velocity components, respectively; the tilde denotes the Favre (density-weighted) average, the superscript $''$ denotes the Favre fluctuation, and the overbar denotes the Reynolds average.

Following the convention, W_{uv} is normalized with respect to the mean wall shear stress at the local x position. Figure 7 displays the wall-normal W_{uv}^+ profiles at three x locations (see Figure 5 for the definition of x) for the three ramps, compared with that of the equilibrium TBL at $x = -35$ mm. In the bulk of the equilibrium TBL, one finds that W_{uv}^+ is smaller than unity and decreases monotonically with increasing distance from the wall. In contrast, there are huge increments for the W_{uv}^+ profiles on the ramps (Figure 7). For example, the maximum W_{uv}^+ is about 16 for $x = 21$ mm of the 24° ramp. The amplification of the Reynolds stress increases with increasing ramp angles owing to increasing interaction strength. For all of the ramps, the Reynolds stresses decay in the streamwise direction, showing relaxation of the perturbed TBLs. Another remarkable difference is that, in the bulk flow of the relaxation TBLs, W_{uv}^+ first increases with the distance from the wall and reaches a peak near the half height of the boundary layer thickness, and then decreases and vanishes near the boundary layer edge. This is due to the strong turbulence shedding from the corner region and occupying the bulk of the relaxation TBLs, as shown in the previous section. Similar outer peaks can be found in the equilibrium TBLs with strong adverse pressure gradients [43]. The difference is that, in the current case, the strong turbulent fluctuations largely originate from the corner region with strong shock-wave/boundary-layer interaction, but in the latter, they are solely due to the adverse pressure gradient. Nevertheless, both cases have a common nature of the pressure-induced redistribution of the turbulent intensity.

In order to quantify the relaxation TBL, we choose to investigate the excess Reynolds stress, which is defined by subtracting the Reynolds stress of the equilibrium TBL out of the relaxation TBL. Spina et al. [44] have concluded that W_{uv}^+ in the bulk of equilibrium TBL is invariant with respect to the Mach number, Reynolds number, and wall temperature. Thus, we simply subtract the $W_{uv}^+(-35)$ profile (at $x = -35$ mm) from $W_{uv}^+(x)$ at all x locations throughout the relaxation TBL. Note that, in the current simulation, the equilibrium W_{uv}^+ is small compared to $W_{uv}^+(x)$ in the relaxation TBL, thus the excess W_{uv}^+ profiles are similar to the original W_{uv}^+ profiles shown in Figure 7.

Unlike the Reynolds stress, more complexities appear when deriving the turbulent heat flux profile of a specific equilibrium TBL. We first need to seek a proper normalization of the turbulent heat flux. The isothermal wall condition has been applied in the current simulation. An attempt to use the wall heat flux to normalize the turbulent heat flux, as displayed in Figure 8(a), shows significant scatter in the near-wall region ($10 < y^+ < 200$). In this case, it is difficult to determine the magnitude of the final equilibrium turbulent heat flux to be subtracted from the relaxation turbulent heat flux.

Note that, for the present simulations, there is a distinct

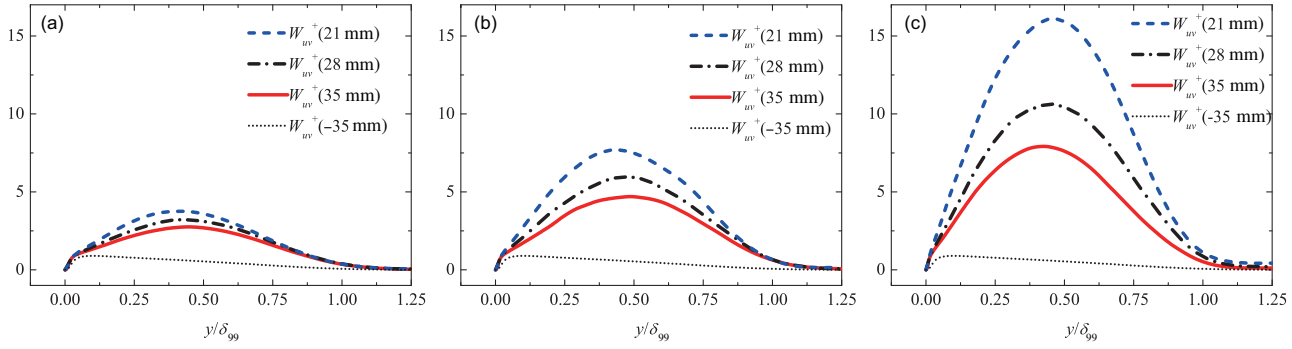

Figure 7 (Color online) Reynolds stress profiles at different x locations on the ramps of angle (a) 14°, (b) 20° and (c) 24°. The Reynolds stress of the equilibrium TBL at $x = -35$ mm is also plotted for comparison.

peak in the molecular heat flux profile at about y^+=6 in the viscous sublayer, owing to the rapid change in mean temperature there in supersonic TBLs with wall temperatures close to the adiabatic case. This peak heat flux is apparently larger than the wall heat flux and has significant scatter. If this local peak magnitude is used as an alternative reference heat flux to normalize the turbulent heat flux (denoted by $W^{\#}_{\Theta}$), as shown in Figure 8(b), we find a better data collapse in the near-wall region. We then postulate that the turbulent heat fluxes of equilibrium TBLs become self-similar under the normalization with respect to the near-wall peak value (which may fluctuate with strongly cooled or heated walls). Then, we subtract the $W^{\#}_{\Theta}(-35)$ profile from $W^{\#}_{\Theta}(x)$ at all x locations throughout the relaxation TBL to get the excess $W^{\#}_{\Theta}$. Again, note that the equilibrium $W^{\#}_{\Theta}(-35)$ is small compared to the relaxation $W^{\#}_{\Theta}$.

To compare with Figure 7, the $W^{\#}_{\Theta}$ profiles are shown in Figure 9 for different x locations and for all of the ramps. One sees that $W^{\#}_{\Theta}$ behaves similarly to W^{+}_{uv}, revealing large amplifications of $W^{\#}_{\Theta}$, increasing with increasing ramp angles, in the bulk flows of the relaxation TBLs. Also, $W^{\#}_{\Theta}$ reaches its peak at about the half-height of the boundary layer thickness, and decays in the streamwise direction in a similar way to W^{+}_{uv}.

3.2 Beta distribution for the excess Reynolds stress and turbulent heat flux

Chen et al. [24] have discovered that, for canonical incompressible TBLs, the defect total stress (or Reynolds stress in the bulk) obeys a power law with respect to the wall distance, owing to the dilation symmetry in the presence of the nonslip wall, as a result of the self-organization. It is interesting to examine whether the dilation symmetry still prevails (or, the turbulence remains to be self-organized) when the relaxation TBL is far from equilibrium.

In the wall-normal direction, the mean flow in the relaxation TBL is in fact quasiparallel between the ramp surface and the free stream. This is evidence that the dilation symmetry imposed by the wall is preserved. According to Chen et al. [24], two dilation centers emerge in the TBL, one at the wall and the other at the edge of the TBL. Consequently, one can construct a dual-power-law:

$$f(y/\delta_r) = A\left(\frac{y}{\delta_r}\right)^{\alpha-1}\left(1-\frac{y}{\delta_r}\right)^{\beta-1}, \quad (1)$$

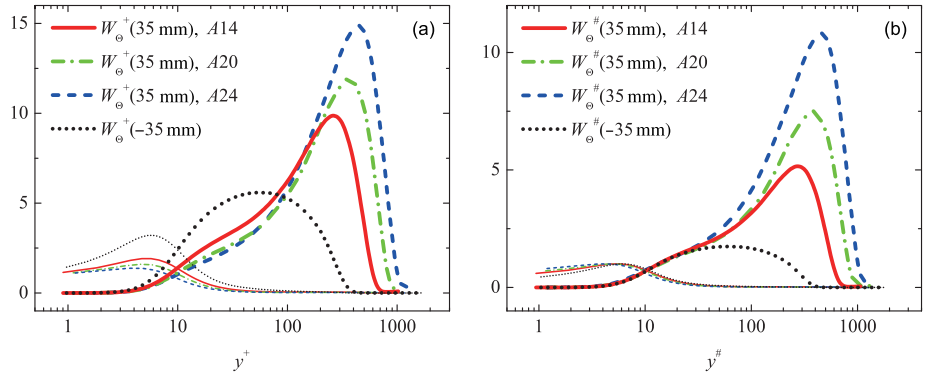

Figure 8 (Color online) Profiles of the turbulent (thick lines) and molecular (thin lines) heat fluxes normalized with respect to the mean wall heat flux (a), and the peak molecular heat flux (b) in the viscous sublayer. The profiles are acquired at x = 35 mm for all of the three ramps and compared with those of the equilibrium TBL at x = −35 mm.

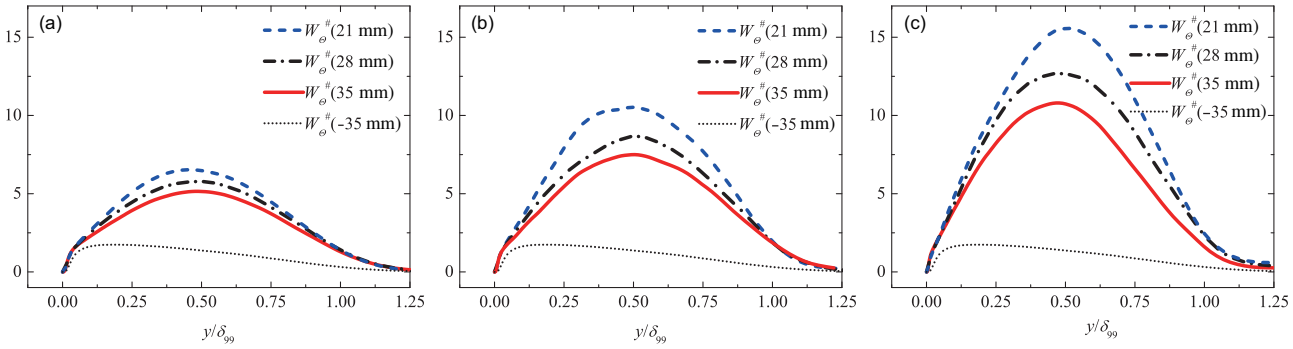

Figure 9 (Color online) Turbulent heat flux profiles at different x locations on the ramps of angles 14° (a), 20° (b), and 24° (c). The turbulent heat flux of the equilibrium TBL at x = −35 mm is also plotted for comparison.

where A is a proportionality coefficient, δ_r is the boundary layer edge, $\alpha-1$ and $\beta-1$ are the scaling exponents quantifying the power laws with respect to the distances from the ramp surface and the outer dilation center (i.e., δ_r), respectively. Note that this dual-power-law provides an opportunity for describing the non-monotonic variations of the excess W^+_{uv} and $W^{\#}_{\Theta}$ in the relaxation TBL. The f function, if normalized with respect to its integration through the boundary layer (e.g., from 0 to 1), is simply the so-called β-distribution:

$$P(\xi,\alpha,\beta)=\frac{\xi^{\alpha-1}(1-\xi)^{\beta-1}}{Beta(\alpha,\beta)}, \tag{2}$$

where $Beta(\alpha,\beta)=\frac{\Gamma(\alpha)\Gamma(\beta)}{\Gamma(\alpha+\beta)}$ is the β function, and $\Gamma(\alpha)=\int_0^{+\infty}t^{\alpha-1}\mathrm{e}^{-t}\mathrm{d}t$ is the gamma function. The β-distribution is known as a continuous probability density function defined on the interval $[0,1]$ and with α and β defining its shape.

Below, we validate the β-distribution for the wall-normal profiles of the excess W^+_{uv} and $W^{\#}_{\Theta}$ of the relaxation TBLs. To determine the parameters in the β-distribution, we have used the least squares method. We find that δ_r can be set to $1.25\delta_{99}$ (δ_{99} is the commonly defined boundary layer thickness, where the mean velocity is 99% of the free stream mean velocity) and is adequate for all simulated cases for different ramp angles and at all streamwise locations, while α and β are varied. To measure α and β with the least squares method, we set $\xi=y/\delta_r$, and normalize W^+_{uv} and $W^{\#}_{\Theta}$ with their integrations in $[0,y/\delta_r]$, denoted by $W^+_{uv,d}$ and $W^{\#}_{\Theta,d}$, respectively. The results are shown in Figure 10 for the 24° ramp, as examples. To be consistent with Figures 7 and 9, the excess W^+_{uv} and $W^{\#}_{\Theta}$ are plotted in the dimensionless coordinate y/δ with the β-distribution (or eq. (1)). Indeed, with appropriate values of α and β, the β-distribution accurately describes the DNS data for both the excess Reynolds stress and turbulent heat flux, and at all streamwise locations. Similar results can be found for the other ramps. It is then interesting to see how α and β vary in the streamwise direction for different cases, as shown below.

3.3 Streamwise development

We have measured the shape factors α and β (which give the scaling exponents by subtracting 1) in the β-distribution for $W^+_{uv,d}$ and $W^{\#}_{\Theta,d}$ at different x locations of the three ramps, as shown in Figure 11.

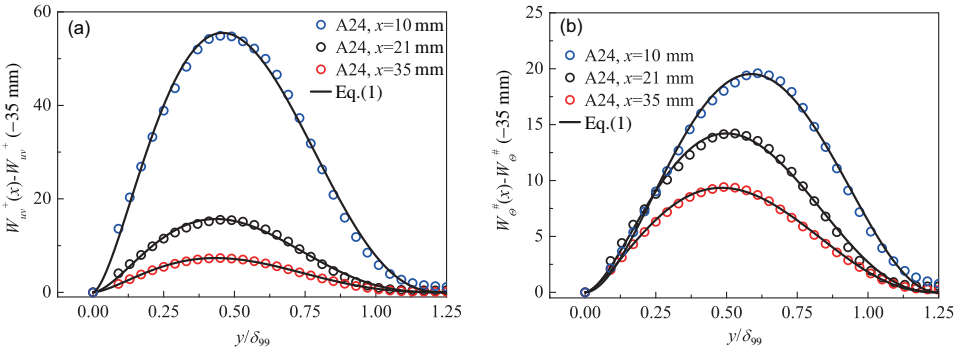

Figure 10 (Color online) DNS-measured excess Reynolds stress (a) and excess turbulent heat flux (b) profiles at different x locations on the 24° ramp compared with the dual-power-law f (or β-distribution).

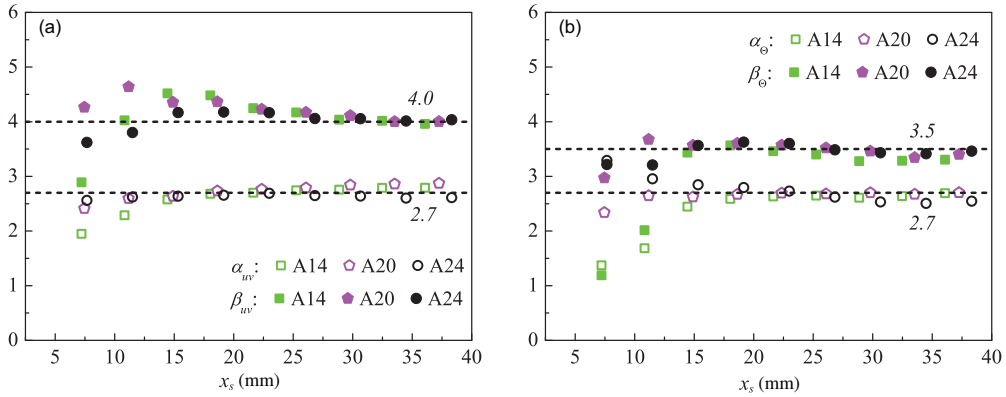

Figure 11 (Color online) Streamwise developments of α and β for the excess Reynolds stresses (a) and excess turbulent (b) heat fluxes of the 14°, 20°, and 24° ramps. The horizontal coordinate x_s denotes the distance from the corner along the ramp. Dashed lines indicate the convergence of α and β in the streamwise direction.

It is surprising that α and β quickly evolve to constants such that both the $W^{+}_{uv,d}$ and $W^{\#}_{\Theta,d}$ profiles become self-similar from the very beginning of the relaxation TBL. Also surprising is the invariance of the ultimate shapes of the profiles with respect to the ramp angles. The ultimate α and β are 2.7 for both W^{+}_{uv} and $W^{\#}_{\Theta}$; the ultimate β is 4.0 for W^{+}_{uv} and 3.5 for $W^{\#}_{\Theta}$, respectively. Note that the ultimate β of $W^{\#}_{\Theta}$ is slightly smaller than that of W^{+}_{uv}. This gives a fuller profile for $W^{\#}_{\Theta}$ near the outer edge of the relaxation TBL, probably owing to the different efficiencies in the momentum and heat transports by eddies.

It is important to examine the decay rates of the integrated excess W^{+}_{uv} and $W^{\#}_{\Theta}$, denoted by Λ^{+} (the total excess Reynolds stress) and $\Omega^{\#}$ (the total excess turbulent heat flux), respectively. Their decays in the streamwise direction are displayed in Figure 12 with the log-log plot for all three ramps. One observes a power-law decay in both quantities (Λ^{+} and $\Omega^{\#}$), which is an additional evidence that the relaxation TBLs are self-organized to preserve the streamwise dilation symmetry, in addition to the wall-normal dilation symmetry shown above. The scaling exponents of the decay seem to be ramp-angle-dependent. For Λ^{+}, the scaling exponents are about –0.5, –1.0, and –1.5 for the three ramp angles (14°, 20°, and 24°), respectively; for $\Omega^{\#}$, they are –0.5, –0.6, and –0.7. These values quantify, in our view, the relaxation TBL, and it will be interesting to examine its universality with more data.

Finally, a further validation of the self-preservation is demonstrated in Figure 13. Indeed, the DNS data of the $W^{+}_{uv,d}$ and $W^{\#}_{\Theta,d}$ profiles at different x locations and for all ramps collapse to the corresponding β-distributions with the above-mentioned ultimate α and β. The peak locations in Figure 13 are given by $\frac{\alpha-1}{\alpha+\beta-2}$ owing to the β-distribution, which are at $y/\delta_r \approx 0.36$ and 0.4 (or $y/\delta_{99} \approx 0.45$ and 0.5) for $W^{+}_{uv,d}$ and $W^{\#}_{\Theta,d}$, respectively.

4 Discussions and conclusions

In their review [4], Smits and Wood identified three levels of complexity in a perturbed TBL: a simple one where the

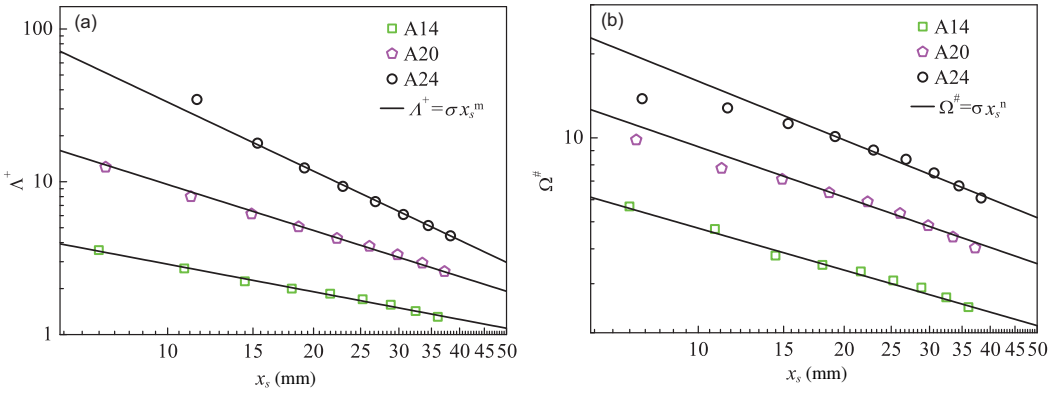

Figure 12 (Color online) Streamwise decays of the total excess Reynolds stresses (a) and total excess turbulent heat fluxes (b) for the 14°, 20°, and 24° ramps. The solid lines show the corresponding power laws.

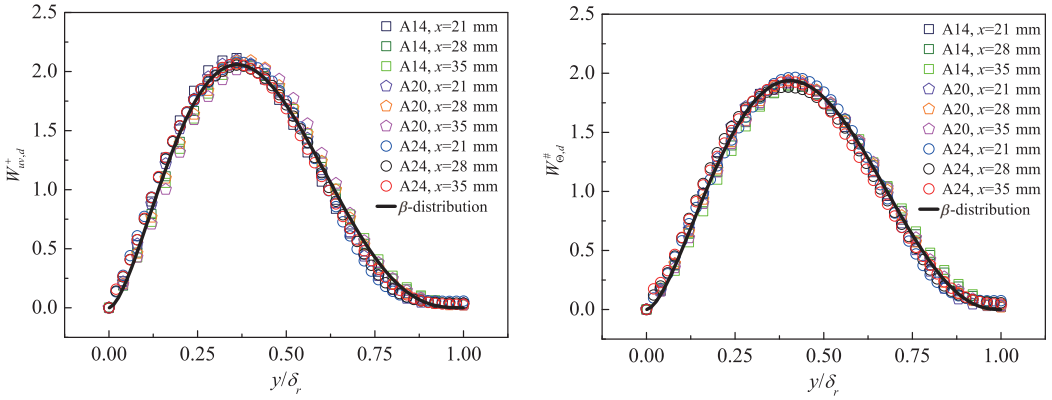

Figure 13 (Color online) In the self-preserving region, for all three ramps. (a) The renormalized excess Reynolds stress ($W^{+}_{uv,d}$) profiles collapse to the β-distribution with α=4 and β=2.7; (b) the renormalized excess turbulent heat flux ($W^{\#}_{\Theta,d}$) profiles collapse to the β-distribution with α=3.5 and β=2.7.

perturbation is so weak that the response exhibits a self-preservation; a more complex one where the perturbation is sudden and severe, and the thin-shear-layer approximation is applicable for practically all of the recovery region; and the most complex one where the boundary layer separates with a significant spatial extension. There is no doubt that compression ramps belong to the second or third level. Compression ramps are also classified by Smits and Wood as complex flows subjected to multiple perturbations [4]. Therefore, it is somewhat astonishing to observe a self-preserving β-distribution in the relaxation TBL of the present compression ramp. This simplicity is important for applications.

We attribute the presently observed self-preservation to the wall-induced dilation symmetry, which is the essential physical mechanism for wall turbulence to be self-organized, whether or not the wall turbulence is in an equilibrium state. In particular, the present findings validate the proposition of She et al. [20, 21, 26] that wall-bounded flows, whether in equilibrium or not, are constrained by the dilation symmetry. A consequence is that one can adopt a new strategy to study complex wall-bounded flows: to identify and quantify the symmetry-related properties of the flow, which have an accurate analytical description for the mean fields in general. We regard this strategy as the most exciting conclusion of this study.

More specific findings are the β-distributions and power-law decays of the excess Reynolds stress and turbulent heat flux in the relaxation TBLs of the compression ramps. These quantifications may be significant for the engineering computations of such flows, which are still a challenge to date [45].

This work was supported by the National Natural Science Foundation of China (Grant Nos. 11452002, 11372008, and 11521091), and the Aeronautical Science Foundation of China (Grant No. 2014ZA71001). The authors thank XinLiang Li (Institute of Mechanics, Chinese Academy of Sciences) for his help on the DNS, which was performed on TianHe-1 at the National Supercomputer Center in Tianjin, China.

1 J. C. Rotta, Prog. Aerospace Sci. **2**, 1 (1962).
2 L. Castillo, and W. K. George, AIAA J. **39**, 41 (2001).
3 D. C. Wilcox, AIAA J. **46**, 2823 (2008).
4 A. J. Smits, and D. H. Wood, Annu. Rev. Fluid Mech. **17**, 321 (1985).
5 P. Bradshaw, and F. Y. F. Wong, J. Fluid Mech. **52**, 113 (1972).
6 H. H. Nigim, Phys. Fluids **8**, 548 (1996).
7 I. P. Castro, and E. Epik, J. Fluid Mech. **374**, 91 (1998).
8 M. P. Escudier, A. Abdel-Hameed, M. W. Johnson, and C. J. Sutcliffe, Exp. Fluids **25**, 491 (1998).
9 D. S. Dolling, AIAA J. **39**, 1517 (2001).
10 H. Babinsky, and J. K. Harvey, *Shock Wave Boundary Layer Interactions* (Cambridge University Press, Cambridge, 2011).
11 M. Jayaram, M. W. Taylor, and A. J. Smits, J. Fluid Mech. **175**, 343 (1987).
12 D. R. Webster, D. B. DeGraaff, and J. K. Eaton, J. Fluid Mech. **323**, 53 (1996).
13 S. E. Belcher, N. Jerram, and J. C. R. Hunt, J. Fluid Mech. **488**, 369 (2003).
14 I. Jacobi, and B. J. McKeon, J. Fluid Mech. **677**, 179 (2011).
15 R. A. Antonia, H. Q. Danh, and A. Prabhu, J. Fluid Mech. **80**, 153 (1977).
16 F. K. Lu, Q. Li, and C. Liu, Prog. Aerospace Sci. **53**, 30 (2012).
17 J. F. Debieve, P. Dupont, D. R. Smith, and A. J. Smits, AIAA J. **35**, 51 (1997).
18 R. A. Antonia, Y. Zhu, and M. Sokolov, Phys. Fluids **7**, 2465 (1995).
19 U. Frisch, *Turbulence: The Legacy of A.N. Kolmogorov* (Cambridge University Press, Cambridge, 2009).
20 Z. S. She, X. Chen, Y. Wu, and F. Hussain, Acta Mech. Sin. **26**, 847 (2010).
21 Z. S. She, X. Chen, and F. Hussain, arxiv: 1112.6312.
22 Z. S. She, Y. Wu, X. Chen, and F. Hussain, New J. Phys. **14**, 093054 (2012).
23 X. Chen, F. Hussain, and Z. S. She, EPL **115**, 34001 (2016).
24 X. Chen, B. B. Wei, F. Hussain, and Z. S. She, Phys. Rev. E **93**, 011102 (2016).
25 X. Chen, and Z. S. She, Sci. China-Phys. Mech. Astron. **59**, 114711 (2016).
26 M. J. Xiao, Z. S. She, in *A Reynolds stress length model for wall turbulence: Proceedings of 69th Annual Meeting of the APS Division of Fluid Dynamics* (Portland, 2016).
27 X. L. Li, D. X. Fu, Y. W. Ma, and X. Liang, Acta Mech. Sin. **26**, 795 (2010).
28 X. L. Li, D. X. Fu, Y. W. Ma, and X. Liang, Sci. China-Phys. Mech. Astron. **53**, 1651 (2010).
29 F. Tong, C. Yu, Z. Tang, and X. Li, Comp. Fluids **149**, 56 (2017).
30 S. Pirozzoli, F. Grasso, and T. B. Gatski, Phys. Fluids **16**, 530 (2004).
31 M. P. Martín, E. M. Taylor, M. Wu, and V. G. Weirs, J. Comp. Phys. **220**, 270 (2006).
32 P. B. Bookey, and C. Wyckham, in *New experimental data of STBLI at DNS/LES accessible Reynolds numbers: Proceedings of 35th AIAA Fluid Dynamics Conference and Exhibit* (Toronto, 2005), pp. 2005-4899.
33 M. Wu, and M. P. Martin, AIAA J. **45**, 879 (2007).
34 F. M. White, *Viscous Fluid Flow* (McGraw-Hill, New York, 2006).
35 Y. Yan, C. Chen, P. Lu, and C. Liu, Aerospace Sci. Tech. **30**, 226 (2013).
36 C. Q. Liu, Y. Q. Wang, Y. Yang, and Z. W. Duan, Sci. China-Phys. Mech. Astron. **59**, 684711 (2016).
37 Y. Andreopoulos, J. H. Agui, and G. Briassulis, Annu. Rev. Fluid Mech. **32**, 309 (2000).
38 J. Délery, and J. P. Dussauge, Shock Waves **19**, 453 (2009).
39 J. C. Anyiwo, and D. M. Bushnell, AIAA J. **20**, 893 (1982).
40 T. A. Zang, M. Y. Hussaini, and D. M. Bushnell, AIAA J. **22**, 13 (1982).
41 G. S. Settles, T. J. Fitzpatrick, and S. M. Bogdonoff, AIAA J. **17**, 579 (1979).
42 P. L. Ardonceau, AIAA J. **22**, 1254 (1984).
43 Z. Harun, J. P. Monty, R. Mathis, and I. Marusic, J. Fluid Mech. **715**, 477 (2013).
44 E. F. Spina, A. J. Smits, and S. K. Robinson, Annu. Rev. Fluid Mech. **26**, 287 (1994).
45 W. W. Liou, G. Huang, and T. H. Shih, Comp. Fluids **29**, 275 (2000).